MULTI-OBJECTIVE OPTIMIZATION OF SCREW CONVEYORS BASED ON NSGA-II ALGORITHM AND ENTROPY-WEIGHTED TOPSIS
/
基于 NSGA-II 算法和熵权 TOPSIS 的螺旋输送机多目标优化

Xiaoyuan ZHANG[1)], TingTing XI[*2)], Baoan WANG[1)], Haikang LI[1)]
[1)] Jinzhong College of Information, Jinzhong 030800, China;
[2)] Shanxi Health Vocational College, Taiyuan 030619, China;
Tel: 0354-5503851; E-mail: xitingting@sxhvc.com
DOI: https://doi.org/10.35633/inmateh-78-58

Keywords: *Screw conveyor; Discrete element method; NSGA-II optimization algorithm; Entropy-weighted TOPSIS; Multi-objective optimization design*

ABSTRACT
To enhance the conveying efficiency of screw conveyors, reduce energy consumption during material transport, and improve particle integrity, this study proposes a multi-objective optimization framework integrating the NSGA-II algorithm with entropy-weighted TOPSIS. Discrete Element Method (DEM) simulations, conducted using EDEM software, and an optimal Latin hypercube sampling design were employed to systematically obtain high-fidelity data on mass flow rate and energy consumption under various operating conditions. A surrogate performance model relating key geometric and operational parameters — including pitch, inclination angle, and rotational speed — to mass flow rate and energy consumption was developed using least squares regression. Subsequently, the NSGA-II algorithm was applied to the surrogate model to generate a Pareto-optimal solution set. The entropy-weighted TOPSIS method was then used to rank and identify the optimal compromise solution from the Pareto frontier. Experimental validation of the optimized design demonstrated significant improvements: the mass flow rate increased by 15.77%, energy consumption decreased by 26.16%, and particle degradation was considerably reduced. These results provide practical, data-driven guidance for the rational design and energy-efficient operation of screw conveyors.

摘要
为了提高螺旋输送机的输送效率，减少螺旋输送机运输过程中的能量消耗，提高颗粒完整度。本文提出了一种基于 NSGA-II 算法和熵权 TOPSIS 的螺旋输送机多目标优化方法。基于离散元软件 EDEM、最优拉丁超立方试验设计，得到螺旋输送机的质量流量、能量消耗数据。基于最小二乘法建立螺距、倾斜角度、螺旋转速与质量流量、能量消耗的性能指标模型。随后使用 NSGA-II 算法从性能指标模型中获参数的最佳值，获得 Pareto 前沿解集，基于熵权 TOPSIS 方法对 Pareto 前沿解集寻优，获得最优解。优化设计的实验验证表明，该设计取得了显著改进：质量流量提高了 15.77%，能量消耗减少了 26.16%。本研究结果为螺旋输送机的设计提供了一定的参考。

INTRODUCTION
Screw conveyors play a critical role in grain processing and transport — but current designs rely heavily on empirical formulas and idealized assumptions, leading to low conveying efficiency, high energy consumption, and poor operational reliability, with no rigorous, science-based design methodology. *Chen et al., (2024),* studied screw conveyor mass flow rate characteristics and hopper–conveyor coupling, achieving high predictive accuracy by integrating experiments and theory—validating the model's precision and reliability. *Sun (2021),* used the SIEM wear model to investigate non-spherical particle transport in horizontal screw conveyors, finding that higher shape indices increase fragmentation risk during particle–wall collisions. *Ma et al., (2024),* developed a novel screw conveyor with concave bi-directional non-symmetric (BNS) blades and conducted DEM simulations in EDEM. Simulation-experiment comparisons showed that this blade geometry significantly alters particle flow patterns, markedly improving conveying performance.

Xiaoyuan ZHANG, Associate Professor; TingTing XI, Lecturer; Baoan WANG, lecturer; Haikang LI, lecturer

Tian et al., *(2018),* proposed a screw conveyor with flexible discrete blades to reduce particle accumulation in the annular gap between the screw and pipe wall; experiments showed blade diameter is proportional to power consumption. *Zhang et al.*, *(2024),* developed a repose angle measurement method and used EDEM to study the influence of model parameters on the repose angle. The simulated and experimental results showed good agreement, validating the robustness and reliability of the method. *Ma et al. (2022)* designed an efficient surrogate-assisted multi-objective optimization framework for permanent magnet vernier machines using a multi-criteria optimal Latin Hypercube Design (LHD). The optimized LHD reduced the number of required finite element analyzes and significantly improved optimization efficiency.

Silva et al., *(2016),* applied NSGA-II to optimize water-flooded oil field operations, improving oil production efficiency. *Huang et al.*, *(2020),* combined Kriging surrogate modeling with NSGA-II to multi-objectively optimize mechanical camellia seed extraction for yield and quality, yielding a Pareto frontier satisfying all design objectives. *Juan C. et al.*, *(2023),* used NSGA-II to optimize 6-DOF trajectories for material deposition, reducing surface underfill and coating volume error by 70%. *Jiang et al.*, *(2021),* proposed a multi-objective lightweight design framework for dump truck bodies, combining NSGA-II with entropy-weighted TOPSIS (Technique for Order Preference by Similarity to Ideal Solution) — reducing body mass by 3.7% without sacrificing structural integrity. *Podder et al.*, *(2021),* applied the same NSGA-II–TOPSIS hybrid to jointly improve peak thermal and electrical efficiencies of a compact PV-T water collector. *Gheibollahi et al.*, *(2023),* extended it to active seat suspension systems, optimizing dynamic performance and significantly enhancing ride comfort.

In this study, pitch, inclination angle, and rotational speed were selected as key design variables. Mass flow rate and energy consumption of the screw conveyor were modeled via least-squares regression fitted to EDEM-based discrete element method (DEM) simulations. A multi-objective optimization was performed to simultaneously maximize mass flow rate and minimize energy consumption. NSGA-II generated the Pareto-optimal set, and entropy-weighted TOPSIS ranked solutions to identify the best balanced compromise. The work systematically examines the individual and coupled effects of the three variables on conveyor performance, yielding quantitative insights into transport mechanisms—and actionable guidance for rational design and industrial deployment of screw conveyors.

MATERIALS AND METHODS

Soybeans exhibit no adhesion under dry environmental conditions. To better replicate the soybean transportation process in discrete element simulations, appropriate contact models must be selected based on the specific particle representation and simulation framework employed. For improved accuracy and computational efficiency in simulating soybean transport, the Hertz–Mindlin no-slip contact model is adopted.

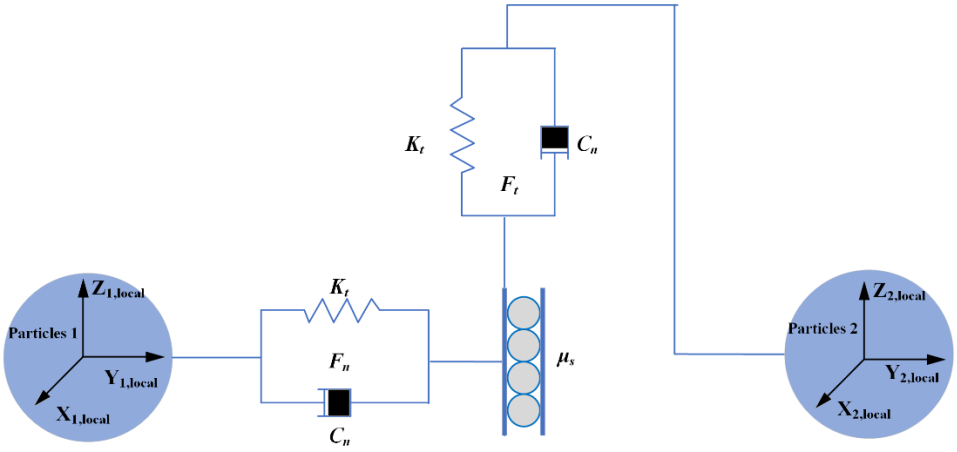

Fig. 1 - Hertz-Mindlin No-Slip Contact Model
(*Zhang X. et al, 2024*)

Suppose that the particle rad_{ii} of sphere 1 and sphere 2 are R_1, R_2 respectively. After elastic contact occurs, the normal overlap amount is α:

$$\alpha = R_1 + R_2 - \left|\vec{r}_1 - \vec{r}_2\right| \tag{1}$$

In the formula: $\vec{r}_2$ are the central position vectors of particles 1 and 2.

The contact radius a of the contact surface of the spherical ball is:

$$a = \sqrt{\alpha R^*} \tag{2}$$

$$\frac{1}{R^*} = \frac{1}{R_1} + \frac{1}{R_2} \tag{3}$$

where: $R*$ is the equivalent radius.

$$F_n = \frac{4}{3} E^* (R^*)^{\frac{1}{2}} \alpha^{\frac{3}{2}} \tag{4}$$

where: F_n is the normal force between particles, $E*$ is the equivalent elastic model, that is, the equivalent elastic modulus. The adhesion on the surface of the particles is not considered.

$$\frac{1}{E^*} = \frac{1-\nu_1^2}{E_1} + \frac{1-\nu_2^2}{E_2} \tag{5}$$

In the formula: μ_1, E_1, μ_2, E_2 are the Poisson's ratios and elastic moduli of the two contacting particles respectively.

$$F_n^d = -2\sqrt{\frac{5}{6}}\beta\sqrt{S_n m^*}\,\overline{v_n^{rel}} \tag{6}$$

where: S_n is the normal stiffness, $m*$ is the equivalent mass, $\overline{v_n^{rel}}$ is the normal component of the relative velocity, β is the damping ratio.

$$\begin{cases} m^* = \dfrac{m_1 \cdot m_2}{m_1 + m_2} \\ \overline{v_n^{rel}} = \left(\vec{v_1} - \vec{v_2}\right) \cdot \dfrac{\vec{r_1} - \vec{r_2}}{\left|\vec{r_1} - \vec{r_2}\right|} \\ \beta = \dfrac{\ln e}{\sqrt{\ln^2 e + \pi^2}} \\ S_n = 2E^*\sqrt{R^*\alpha} \end{cases} \tag{7}$$

where: e is the coefficient of restitution. $\vec{v_1}$, $\vec{v_2}$ is the velocity of the two particles before the collision.

$$\begin{cases} F_\tau = -S_\tau \delta \\ F_\tau^d = -2\sqrt{\dfrac{5}{6}}\beta\sqrt{S_\tau m^*}\,\overline{v_\tau^{vel}} \end{cases} \tag{8}$$

where: F_τ is the tangential force between particles, F_τ^d is the tangential damping force. S_τ is the tangential stiffness, δ_τ is the tangential overlap amount. $\overline{v_\tau^{vel}}$ is the tangential component of the relative velocity.

$$\begin{cases} S_\tau = 8G^*\sqrt{R^*\alpha} \\ G^* = \dfrac{2-\mu_1^2}{G_1} + \dfrac{2-\mu_2^2}{G_2} \end{cases} \tag{9}$$

where: $G*$ is the equivalent shear modulus. G_1, G_2 is the shear modulus of the two colliding particles.

The frictional force F_f is related to the tangential force.

$$F_f = \mu_s F_n \tag{10}$$

where: μ_s is the coefficient of static friction.

$$T_i = -\mu_r F_n R_i \omega_i \tag{11}$$

where: μ_r is the coefficient of rolling friction; R_i is the distance from the contact point to the center of mass; ω_i is the angular velocity vector of the material particle at the contact point.

Since the Hertz-Mindlin (no-slip) contact model offers both high computational efficiency and accuracy in force calculation, and given the large number of particle interactions in the screw conveyor-under identical time-step sizes and contact stiffness-the Hertz-Mindlin (no-slip) contact model is adopted.

Hard-sphere and soft-sphere models are the most widely used simplified particle models. The hard-sphere model suits instantaneous collisions under low-concentration, high-velocity conditions, whereas the soft-sphere model offers greater flexibility for complex operational conditions. This paper adopts the soft-particle contact model, as shown in Figure 2.

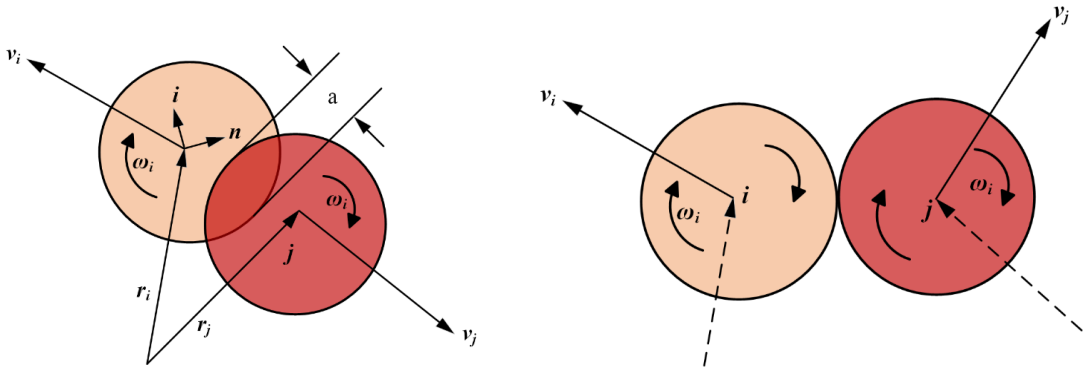

(a) Soft Sphere Model (b) Hard Sphere Model

Fig. 2 - Schematic Diagram of the Sphere Model

MFR represents the mass flow rate, ED represents the energy consumption. x_i (i=1, 2, …. n) are the system parameters. The coefficients a_0, b_0, a_i, b_i, a_{ii}, b_{ii}, a_{ij}, b_{ij} are unknown parameters determined through experimental design and the least squares method.

$$MFR = a_0 + \sum_{i=1}^{n} a_i x_i + \sum_{i=1}^{n} a_{ii} x_i^2 + \sum_{1=i<j}^{n} a_{ij} x_i x_j$$
$$ED = b_0 + \sum_{i=1}^{n} b_i x_i + \sum_{i=1}^{n} b_{ii} x_i^2 + \sum_{1=i<j}^{n} b_{ij} x_i x_j \quad (12)$$

To enable more robust global analysis and enhance the accuracy of computational results, this study optimizes the distribution space of data points—based on Latin hypercube sampling—so that the sampled points are both more uniformly and more densely distributed across the design space. Accordingly, an optimal Latin hypercube experimental design is adopted for data sampling in this paper.

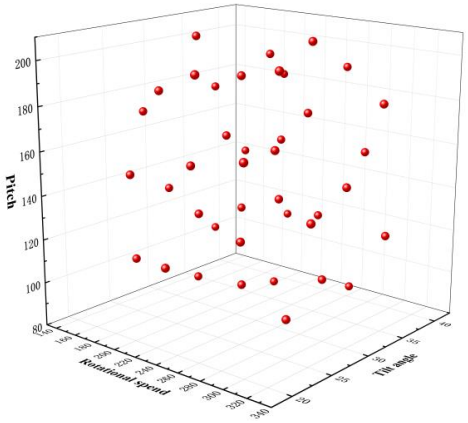

Fig. 3 - The uniformly distributed test points generated by the optimal Latin hypercube sampling method

The multi-objective optimization design procedure for screw conveyors can be summarized as follows:

(1) Define the system parameters and identify the key design variables for optimization.

(2) Develop a three-dimensional geometric model of the screw conveyor and perform discrete element method (DEM) simulations using EDEM. Employ an optimal Latin hypercube sampling strategy to generate representative design points; subsequently, conduct EDEM simulations at these points to obtain corresponding performance data.

(3) Establish surrogate models—using the least squares method—to describe the mapping relationships between critical design variables (i.e., pitch, inclination angle, and rotational speed) and objective responses (i.e., mass flow rate and energy consumption). Perform both univariate and multivariate sensitivity analyzes to quantify the influence of each parameter on the objectives and elucidate their underlying functional relationships.

(4) Apply a multi-objective optimization framework based on the Non-dominated Sorting Genetic Algorithm II (NSGA-II) to compute the Pareto frontier.

(5) Integrate entropy-weighted TOPSIS (Technique for Order Preference by Similarity to Ideal Solution) analysis to objectively determine the relative weights of performance indicators and thereby select the most balanced compromise solution from the Pareto frontier.

A flowchart illustrating the proposed multi-objective optimization design process is presented in Fig. 4.

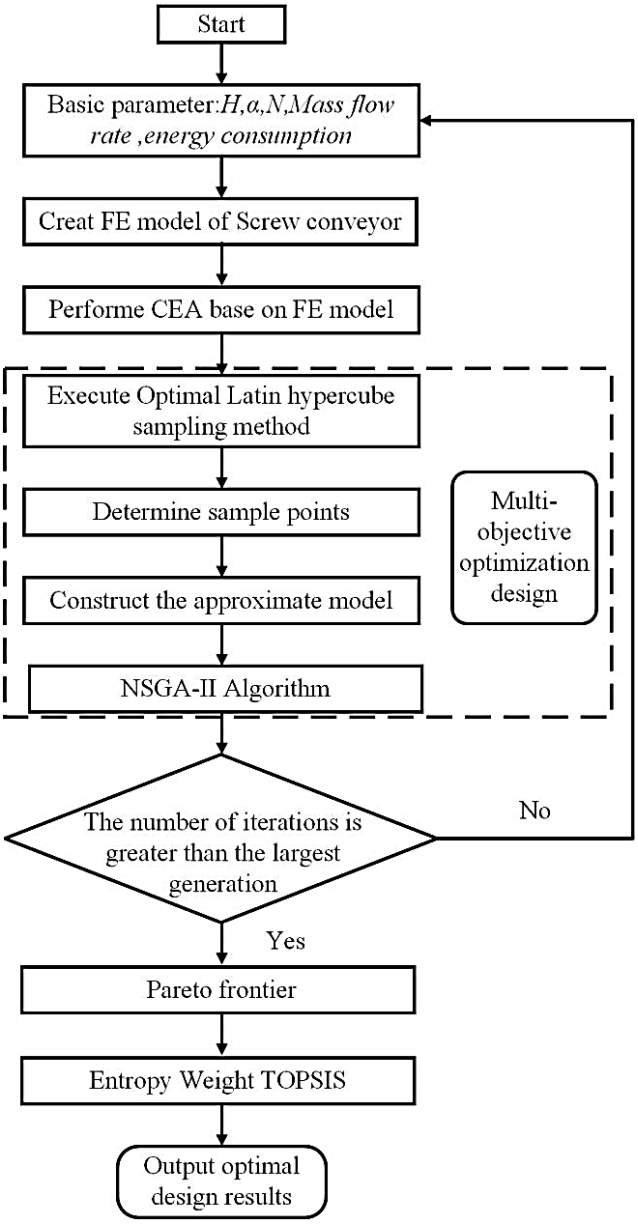

Fig. 4 - Flow chart of multi-objective optimization procedure

FINITE ELEMENT MODEL AND ANALYSIS

The screw conveyor comprises a screw shaft and housing. A 3D parametric model of both components is built in SOLIDWORKS, with key structural parameters specified. The assembled geometry is imported into EDEM for discretization, generating a mesh of 747,040 elements. Rigorous quality checks—assessing aspect ratio, skewness, and continuity—are performed to ensure geometric fidelity and numerical robustness. A dedicated high-performance workstation is used to enable efficient, high-fidelity discrete element simulations.

As shown in Figure 5, the system uses an inclined screw conveyor. During particle transport, each particle experiences concurrent forces: thrust from the rotating screw flights, inter-particle contact forces (normal and tangential), and wall friction. Consequently, the force balance on each particle is highly nonlinear and governed by coupled factors—including particle size distribution, material properties, fill level, rotational speed, and inclination angle.

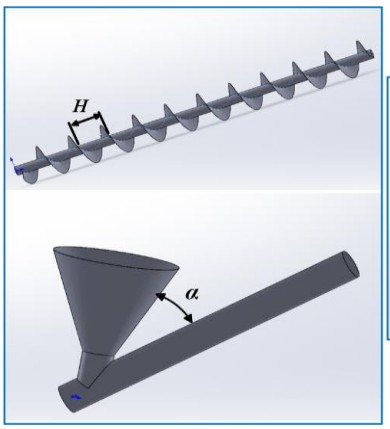

Fig. 5 - Structural Diagram of the Screw Conveyor

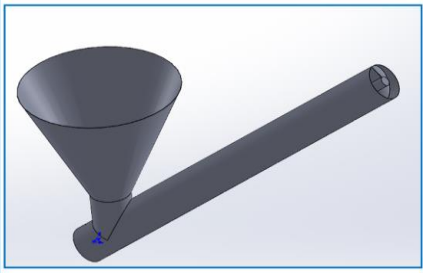

Fig. 6 - Soybean Particle Model

Taking the transport of soybean particles as an example, appropriate geometric parameters for the soybean model were determined based on physical measurements of soybean samples. Specifically, the particles were modeled as spheres with a diameter of 10 mm. A particle simulation model was then developed to reflect the actual shape of soybeans, and the resulting soybean simulation particle model is presented in Figure 6.

A specific type of screw conveyor, illustrated in Figure 1, was selected for analysis. Based on the engineering data reported by *Zhou (2019)*, the pitch H, inclination angle α, and rotational speed N were considered as interval variables, with their ranges provided in Table 1 and Figure 5. The parameter values listed in Tables 1 and 2 were derived from established engineering practice. For each parameter, the midpoint of the corresponding interval was selected as the nominal value. The optimization intervals were defined as [160 mm, 320 mm] for the pitch, [20°, 40°] for the inclination angle, and [90r/min, 210r/min] for the rotational speed. The material properties used in the screw conveyor simulation are presented in Table 3.

Table 1

Optimized Parameters

Parameter	Value	Parameter	Value
Pitch H (mm)	[160,320]	Rotational speed N (r/min)	[90,210]
Inclination angle α (°)	[20,40]		

Table 2

Structural Parameters of the Screw Conveyor

Parameter	Value	Parameter	Value
Diameter of the screw shaft D_0, mm	140	Clearance C between the screw blade and the pipe wall C, mm	5
Diameter of the screw blade D, mm	500	Inner diameter of the screw barrel wall, mm	510
Thickness of the screw blade t_s, mm	4	Outer diameter of the screw barrel wall, mm	518

Table 3

Parameter Selection for the Simulation Experiment

(Zhang T. et al, 2017)

Parameter	Value	Parameter	Value
Poisson's ratio of soybeans	0.25	Restitution coefficient (soybean–soybean)	0.6
Poisson's ratio of steel	0.3	Restitution coefficient (soybean–steel)	0.6
Shear modulus of soybeans Pa	$1.0\times e^{7}$	Static friction coefficient (soybean–soybean)	0.45
Shear modulus of steel Pa	$2.06\times e^{11}$	Static friction coefficient (soybean–steel)	0.3
Density of soybeans (kg/m^3)	1228	Rolling friction coefficient (soybean–soybean)	0.05
Density of steel (kg/m^3)	7850	Rolling friction coefficient (soybean–steel)	0.01

In order to make the data points more evenly and densely distributed in the spatial distribution, according to the optimal Latin hypercube experimental design, a simulation data sample is established, as shown in Table 4.

Table 4

Data Distribution Points

Run#	X_1	X_2	X_3	Mass flow rate	Energy consumption
1	229.74	20	117.69	85.6	475.5
2	164.1	34.87	108.46	103.4	920.7
3	278.97	26.67	166.92	61.8	490.8
4	254.36	36.41	123.85	92.5	873.7
5	196.92	40	182.31	76	832.2
			.....		
36	246.15	27.18	102.31	95.5	654.6
37	168.21	28.21	136.15	95.2	670.0
38	172.31	33.85	179.23	79.6	744.8
39	291.28	31.28	105.38	94.9	760.3
40	205.13	39.49	114.62	100.7	1021.7

ANALYSIS AND OPTIMIZATION

In this study, the pitch, inclination angle, and rotational speed are selected as input variables, and an optimal Latin hypercube sampling (LHS) design is employed to generate the experimental configurations. The mass flow rate and energy consumption are adopted as output variables. Specifically, the mass flow rate is defined as the mass of conveyed particles per unit time under steady-state conveying conditions in the screw conveyor. Energy consumption is quantified as the total energy dissipated due to inter-particle collisions and particle–wall collisions over a specified time interval.

Univariate Analysis

As shown in Figure 7(a), the plot illustrates the relationships among pitch, mass flow rate, and energy consumption. The influence of pitch on these two performance metrics is analyzed as follows: with increasing pitch, the mass flow rate gradually increases, whereas energy consumption gradually decreases. This trend originates from the fact that a larger pitch enables a greater number of soybeans to be accommodated within a given cross-sectional area of the screw, thereby enhancing conveying capacity and increasing the mass flow rate. Concurrently, the enlarged pitch reduces inter-particle collisions among soybeans, leading to lower energy dissipation *(Minglani D. et al., 2020)*.

Figure 7(b) illustrates the relationships between the inclination angle and both the mass flow rate and energy consumption. The results indicate that, as the inclination angle increases, the mass flow rate gradually decreases while the energy consumption correspondingly increases. This behavior occurs because a larger inclination angle raises the height of the discharge port, thereby increasing the resistance to material transport and reducing the mass flow rate. At the same time, the greater vertical lifting height intensifies the frequency and severity of collisions among soybean particles, which leads to increased energy consumption.

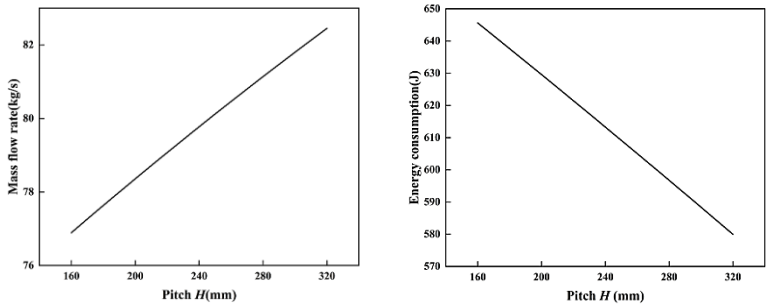

a)

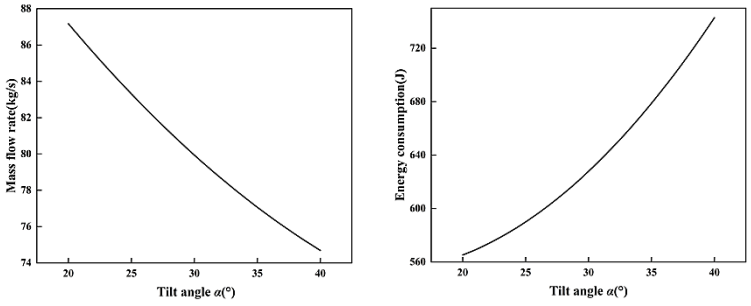

b)

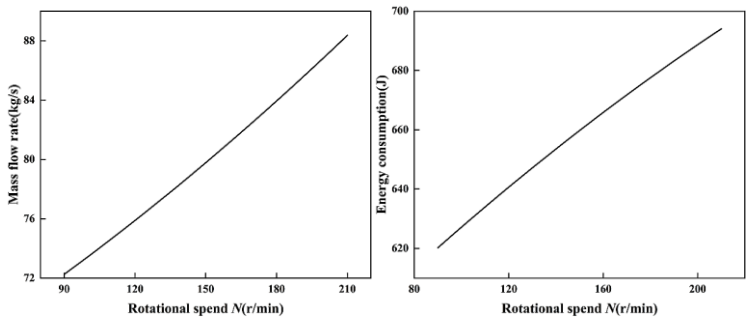

(c)

Fig. 7 - Relationships among pitch, inclination angle, rotational speed, mass flow rate, and energy consumption

Figure 7(c) illustrates the relationships between screw rotational speed and both the mass flow rate and energy consumption. The results show that both the mass flow rate and energy consumption increase monotonically as the rotational speed increases. This occurs because a higher rotational speed enables more soybeans to be transported per unit time, thereby increasing the mass flow rate. Consequently, the frequency and intensity of particle–particle and particle–equipment interactions increase, resulting in higher energy consumption.

Multivariate Analysis

As illustrated in Figure 8, the interrelationships among pitch, inclination angle, rotational speed, mass flow rate, and energy consumption are systematically examined. Because univariate analysis cannot capture interactions among these variables, a multivariate analytical approach is adopted. Three-dimensional visualizations prove especially effective in elucidating complex, coupled dependencies among these parameters. As revealed by the analysis of Figure 7, multiple locally optimal configurations exist for both mass flow rate and energy consumption. To rigorously identify the globally optimal trade-off solution, further investigation is warranted—specifically, a formal multi-objective optimization framework should be implemented.

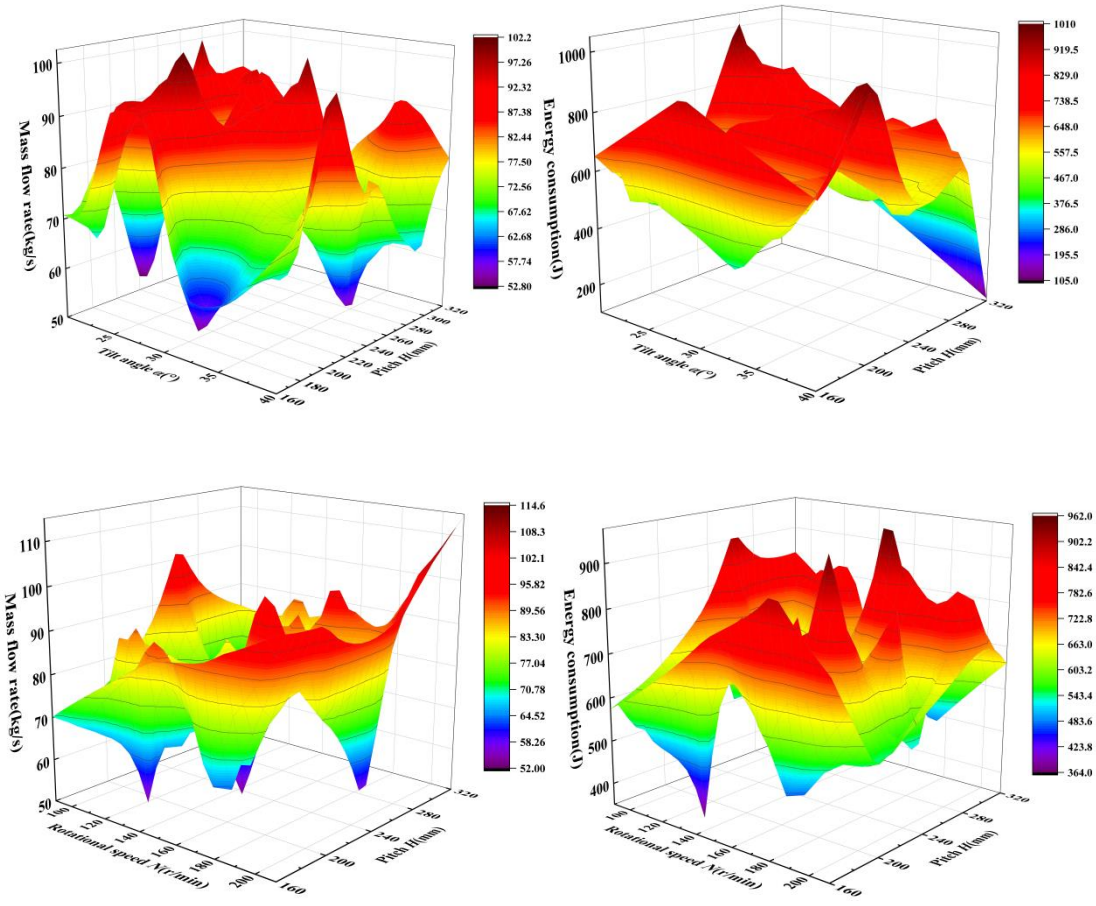

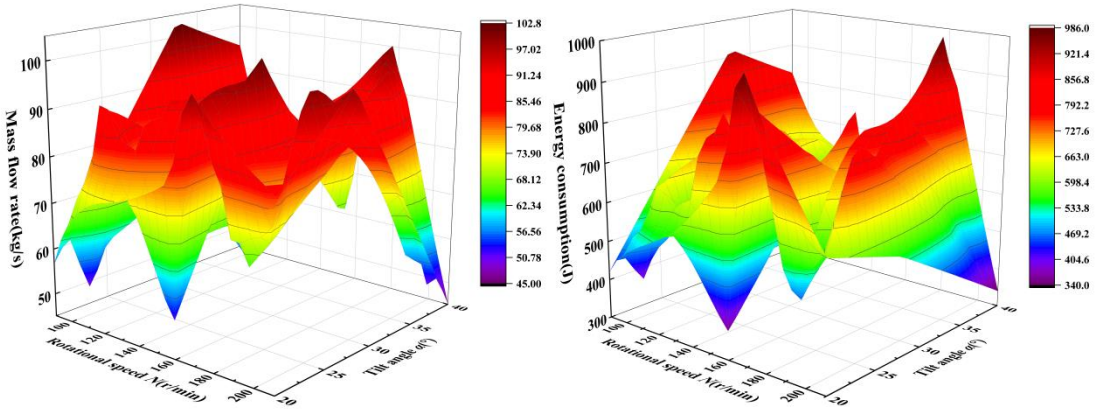

Fig. 8 - Relationships among pitch, inclination angle, rotational speed, mass flow rate, and energy consumption

Multi-objective Optimization Design Based on NSGA-II

To enhance the transportation efficiency of screw conveyors while simultaneously reducing energy consumption, a multi-objective optimization framework is adopted. The genetic algorithm (GA) is inspired by the natural evolutionary principle of "survival of the fittest." By encoding the problem's search space into a genetic representation—typically strings of binary, integer, or real-valued variables—GA facilitates adaptive, population-based, and robust global optimization. Among various GA variants, the Non-dominated Sorting Genetic Algorithm II (NSGA-II) is especially well-suited for multi-objective optimization problems. As an improved successor to the original NSGA, NSGA-II achieves superior computational efficiency and solution quality through two key innovations: fast non-dominated sorting and crowding distance assignment. Specifically, it ensures a well-distributed and convergent approximation of the Pareto front by assigning each individual in the population a non-domination rank (i.e., its frontier level) and computing its crowding distance—a metric that quantifies local solution density in objective space. This mechanism effectively balances diversity preservation and convergence toward the true Pareto-optimal set. Consequently, NSGA-II efficiently identifies a high-quality, uniformly distributed set of non-dominated solutions that collectively approximate the Pareto-optimal solution set. The overall workflow of the algorithm is illustrated in Figure 9.

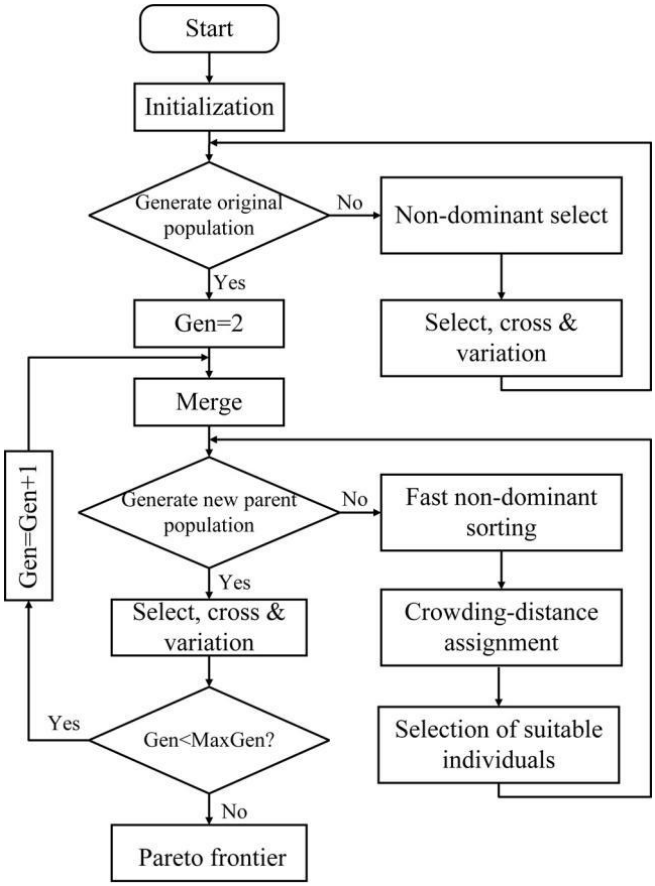

Fig. 9 - Flow Chart of the NSGA–II Algorithm Program

For multi-objective optimization of screw conveyors, both design parameters and performance objectives must be systematically integrated. Design parameter samples are generated via optimal Latin hypercube sampling (LHS). Subsequently, discrete element method (DEM) simulations are performed in EDEM software to obtain quantitative performance data. Finally, a surrogate mathematical model is constructed to characterize the relationships between the design parameters and key performance indicators. The pitch H, inclination angle α and rotational speed N were defined as optimization parameters, with mass flow rate and energy consumption selected as optimization objectives. Assume that H is x_1, α is x_2, and N is x_3; accordingly, the mass flow rate and energy consumption are denoted as $f_1(x)$ and $f_2(x)$ respectively.

$$\begin{aligned} Min \quad & W(x) = [f_1(x), f_2(x),] \\ s.t \quad & 160 \le x_1 \le 320 \\ & 20 \le x_2 \le 40 \\ & 90 \le x_3 \le 210 \end{aligned} \tag{13}$$

The objective functions of the mass flow rate and energy consumption are respectively:

$$\begin{cases} f_1(x_1, x_2, x_3) = 236.1319 - 0.6328x_1 - 0.8669x_2 - 0.5057x_3 + 0.00088x_1^2 \\ \quad + 0.0004x_2^2 + 0.00024x_3^2 + 0.0046x_1x_2 + 0.00314x_2x_3 - 0.00028x_1x_3 \\ f_2(x_1, x_2, x_3) = 261.2959 - 2.313x_1 + 25.3534x_2 + 2.0454x_3 + 0.0047x_1^2 \\ \quad + 0.1836x_2^2 - 0.0031x_3^2 + 0.0045x_1x_2 - 0.0838x_2x_3 - 0.0045x_1x_3 \end{cases} \tag{14}$$

where: $f_1(x_1, x_2, x_3)$ is the objective function of the mass flow rate, and $f_2(x_1, x_2, x_3)$ is the objective function of the energy consumption.

In the screw conveyor system, optimization parameters exhibit disparate physical units and value ranges; therefore, normalization is required for all parameters to ensure comparability and numerical stability during optimization. Each normalized parameter is scaled to lie within the interval [-1, 1]. The nominal (standard) values and corresponding ranges of all parameters are summarized in the Table5.

Table 5

Range of interval variables

Interval variables	Nominal values	Lower bounds	Upper bounds
H/mm	240	160	320
α/°	30	20	40
N/(r/min)	150	90	210

The normalization formula is given below:

$$x_1 = \frac{H - 240}{80}, x_2 = \frac{\alpha - 30}{10}, x_3 = \frac{\mu - 150}{60} \tag{15}$$

where x_i is the normalized parameter.

The multi-objective optimization model of the screw conveyor is as follows:

$$\begin{aligned} & \max f_1(x_1, x_2, x_3) \\ & \min f_2(x_1, x_2, x_3) \\ & s.t. 160 < H < 320 \\ & \quad 20 < \alpha < 40 \\ & \quad 90 < N < 210 \end{aligned} \tag{16}$$

After normalizing Equation (16):

$$\begin{aligned} & \max f_1(x_1, x_2, x_3) \\ & \min f_2(x_1, x_2, x_3) \\ & s.t. X = \left\{ X_1^T \right\}^T \\ & X_1 = \left\{ x_1, x_2, x_3 \right\}^T; x_i \in [-1, 1], i = 1, 2, 3 \end{aligned} \tag{17}$$

where: $f_1(x_1, x_2, x_3)$ is the objective function of the mass flow rate, and $f_2(x_1, x_2, x_3)$ is the objective function of the energy consumption.

The NSGA-II algorithm is well known for its robust global optimization capability and rapid convergence *(Yu R. et al., 2022)*. Owing to its superior performance in solving multi-objective optimization problems, this study adopts NSGA-II to optimize the multi-objective model defined in Equation (17).

For the screw conveyor design problem, transportation efficiency and energy consumption reduction are equally critical objectives. Accordingly, the two objective functions—$f_1(x_1, x_2, x_3)$ and $f_2(x_1, x_2, x_3)$—are assigned equal priority, with a weight ratio of 1:1. The algorithmic parameters are configured as follows: an initial population size of 100, a maximum number of generations of 200, and a crossover probability of 0.9. After 20,000 function evaluations (i.e., 200 generations × 100 individuals), the Pareto frontier is obtained. This Pareto frontier is presented in Figure 10.

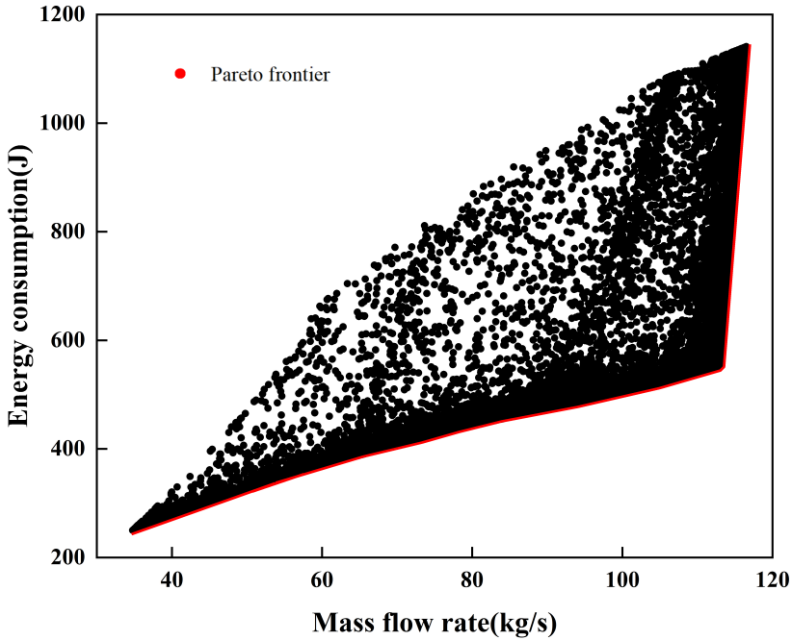

Fig. 10 - Pareto frontier Diagram

In the Pareto frontier of the dual-objective optimization problem shown in Figure 10, the black scatter points represent the feasible solution set generated during the multi-objective optimization process, i.e., solutions that satisfy all constraints. The red curve represents the Pareto optimal solution set, which defines the optimal trade-off boundary between the two objectives. In this study, pitch, inclination angle, and rotational speed are treated as design variables, while mass flow rate and energy consumption are selected as the objective functions. Under the dual-objective optimization framework, a set of solutions is obtained that balances the maximization of mass flow rate and the minimization of energy consumption.

Optimization Search Based on Entropy Weight TOPSIS

The Pareto frontier contains multiple feasible solutions that satisfy the multi-objective optimization requirements. To identify the optimal compromise solution, this study integrates the entropy weight method with the TOPSIS method, combining their respective advantages within an entropy-weighted TOPSIS framework *(Shakouri O. et al., 2021; Bisariya S. et al., 2024)*. This integrated approach enables a comprehensive evaluation of the screw conveyor's mass flow rate and energy consumption, while facilitating a systematic analysis of the Pareto frontier.

The TOPSIS (Technique for Order Preference by Similarity to Ideal Solution) method is widely adopted in multi-objective optimization *(Wang D. et al., 2016; Dao T.P. et al., 2015; Abhilash P.M. et al., 2022)*. It transforms a multi-criteria decision-making problem into a single comprehensive evaluation by measuring the relative distances of alternatives from the ideal and anti-ideal solutions. In contrast, the entropy weight method objectively determines indicator weights based on information entropy, thereby enhancing the objectivity and credibility of the weighting scheme.

By coupling the NSGA-II algorithm with the entropy-weighted TOPSIS method, the proposed framework improves the robustness and reliability of selecting the optimal solution from the Pareto frontier *(Li Y. et al., 2022; Zhou Z. et al., 2025; Ou Z. et al., 2025)*.

From the Pareto-optimal solution set, 2000 representative performance indicator vectors are selected and structured into the decision matrix X required by the TOPSIS method.

$$X = \left(x_{ij}\right)_{nm} = \begin{pmatrix} x_{11} & x_{12} & \cdots & x_{1m} \\ x_{21} & x_{22} & \cdots & x_{2m} \\ \vdots & \vdots & \cdots & \vdots \\ x_{n1} & x_{n2} & \cdots & x_{nm} \end{pmatrix} \quad (18)$$

X is an $n \times m$ matrix, where n denotes the number of candidate design schemes and m denotes the number of performance indicators.

To render X dimensionless, each element undergoes positive transformation followed by standardization. In the multi-objective optimization of screw conveyors, the mass flow rate is a benefit-type objective (i.e., higher values are preferable), whereas energy consumption is a cost-type objective (i.e., lower values are preferable).

$$r_{ij} = \frac{x_{ij} - \min\left\{x_{ij}\right\}}{\max\left\{x_{ij}\right\} - \min\left\{x_{ij}\right\}} \quad (19)$$

$$r_{ij} = \frac{\max\left\{x_{ij}\right\} - x_{ij}}{\max\left\{x_{ij}\right\} - \min\left\{x_{ij}\right\}} \quad (20)$$

The information entropy H_j and the weight coefficient ω_j of each performance indicator were calculated for the multi-objective optimization problem of the screw conveyor.

$$H_j = -\frac{1}{\ln m}\sum_{i=1}^{m} f_{ij} \ln f_{ij} \quad (21)$$

$$f_{ij} = \frac{r_{ij}}{\sum_{i=1}^{m} r_{ij}} \quad (22)$$

$$\omega_j = \frac{1 - H_j}{n - \sum_{j=1}^{n} H_j} \quad (23)$$

where f_{ij} is the characteristic proportion of the i-th scheme under the j-th indicator. The information entropy and associated weight coefficients for each indicator are summarized in Table 6:

Table 6

Weights of Performance Indicators

Performance Indicators	Mass Flow Rate	Energy Consumption
Information Entropy	0.98625	0.98922
Entropy Weight	0.56035	0.43965

Normalization of the decision matrix X is performed as follows:

$$A = [a_{ij}] \quad (24)$$

$$a_{ij} = \frac{x_{ij}}{\sqrt{\sum_{i=1}^{m} x_{ij}^2}} \quad (25)$$

Following the entropy-based weighting procedure applied to the decision matrix X, a weighted decision matrix B is obtained:

$$B = \omega A = \begin{vmatrix} \omega_1 a_{11} & \omega_2 a_{12} & \cdots & \omega_n a_{1n} \\ \omega_1 a_{21} & \omega_2 a_{22} & \cdots & \omega_n a_{2n} \\ \vdots & \vdots & \cdots & \vdots \\ \omega_1 a_{m1} & \omega_2 a_{m2} & \cdots & \omega_n a_{mn} \end{vmatrix} \quad (26)$$

Compute the Euclidean distances between each performance indicator and both the positive and negative ideal solutions, and subsequently assess the relative superiority and inferiority of the alternatives.

$$C^{+} = \begin{cases} \max_{1\leqslant j\leqslant n}\{c_{ij}\} & i \in I_1 \\ \min_{1\leqslant j\leqslant n}\{c_{ij}\} & i \in I_2 \end{cases} \quad (27)$$

$$C^{-} = \begin{cases} \max_{1\leqslant j\leqslant n}\{c_{ij}\} & i \in I_1 \\ \max_{1\leqslant j\leqslant n}\{c_{ij}\} & i \in I_2 \end{cases} \quad (28)$$

where I_1 is a benefit-type indicator; I_2 is a cost-type indicator.

The Euclidean distance is as follows:

$$\begin{cases} D_i^{+} = \sqrt{\sum_{j-1}^{m}\left(c_{ij} - c_j^{+}\right)^2} \\ D_i^{-} = \sqrt{\sum_{j-1}^{m}\left(c_{ij} - c_j^{-}\right)^2} \end{cases} \quad (29)$$

The relative closeness degree is as follows:

$$S_i = \frac{D_i^{-}}{D_i^{+} + D_i^{-}} \quad (30)$$

The relative closeness degree was calculated based on the Euclidean distances to the positive and negative ideal solutions, and the alternatives were subsequently ranked accordingly. This metric ranges from 0 to 1, with higher values indicating superior performance. The optimization results are presented in Table 7. Through comprehensive analysis, the optimal parameter combination for the screw conveyor was determined as follows: pitch =240.6 mm, inclination angle =20°, and screw rotational speed =106.81 r/min.

Table 7

Euclidean Distance and Relative Closeness Degree

Scheme Serial Number	Distance to the Positive Ideal Solution	Distance to the Negative Ideal Solution	Relative Closeness Degree	Ranking
1	0.405140978	0.335151397	0.452728419	18868
2	0.346217211	0.392328713	0.531217762	15295
3	0.460426579	0.383925615	0.454698428	18735
4	0.386812445	0.346217074	0.472309866	17679
…….				

Analysis of the Optimization Results

By simulating the soybean transport process in a screw conveyor, both the mass flow rate and energy consumption were systematically optimized. The corresponding optimization metrics are summarized in Table 8. A comparative analysis of key performance indicators before and after optimization shows that the mass flow rate increased by 15.77%, while energy consumption decreased by 26.16%. These improvements collectively enhance the overall performance of the screw conveyor—thereby achieving simultaneous gains in operational efficiency and environmental sustainability.

Table 8

Comparison of Performance Indicators Before and After Optimization

	Mass Flow Rate	Energy Consumption
Before optimization	76.02	633.10
After optimization	88.01	467.47
Difference/%	15.77%	26.16%

Experimental Verification

The screw conveyor shown in Figure 11 is optimized by using the optimization method proposed in this paper. Experiments are carried out by changing the pitch, inclination angle and rotational speed of the screw conveyor on the basis of the original machine. When the transportation of the screw conveyor is stable, the mass flow rate of the screw conveyor is measured by a flow tester. The trend of the change in energy consumption is indirectly reflected by analyzing the surface damage rate of soybean particles. Before optimization, the mass flow rate was 20.1 kg/min, and after optimization, the mass flow rate was 30.3 kg/min. By sampling and inspecting the surface damage of soybean particles, after optimization, the surface damage rate of soybean particles decreases, and the energy consumption generated by the collision between soybeans decreases.

By using the optimization method proposed in this paper, the mass flow rate of the screw conveyor increases and the energy consumption decreases, which reflects the reliability of this optimization method.

Fig. 11 - The screw conveyor

CONCLUSIONS

1. This study develops a three-dimensional geometric model of a screw conveyor and simulates the conveying process of soybeans using EDEM discrete element software. Uniformly distributed sampling points are generated via the optimal LHS method. Mass flow rate and energy consumption data are extracted from the EDEM simulations. Subsequently, a mathematical model relating key operational parameters—namely, pitch, inclination angle, and screw rotational speed—to the performance metrics (mass flow rate and energy consumption)—is constructed using the least squares method. Finally, the resulting multi-objective optimization problem is solved using MATLAB in conjunction with the non-dominated sorting genetic algorithm II (NSGA-II), yielding a Pareto-optimal solution set that constitutes the Pareto front.

2. To select a single preferred solution from the Pareto frontier, an entropy-weighted TOPSIS method is applied. This transforms the multi-criteria decision-making problem into a unified comprehensive evaluation framework. Performance indicators are first normalized and directionally aligned (i.e., positively oriented), followed by entropy-based weight calculation to objectively quantify the relative importance of each criterion. The optimal design is identified based on minimum Euclidean distance to the ideal solution and maximum relative closeness; the final recommended configuration features a pitch of 240.6 mm, an inclination angle of 20°, and a screw rotational speed of 106.81 r/min.

3. Comparative analysis between pre- and post-optimization performance demonstrates that the proposed multi-objective optimization strategy significantly improves conveyor efficiency: the mass flow rate increases by 15.77%, while energy consumption decreases by 26.16%. These results collectively confirm substantial enhancement in both productivity and energy efficiency of the screw conveyor system.

ACKNOWLEDGEMENT

This research was funded by the Science and Technology Innovation Project for Higher Education Institutions in Shanxi Province (2022L659).

REFERENCES

[1] Abhilash, P. M.; Chakradhar, D. (2022). Multi-Response Optimization of Wire EDM of Inconel 718 Using a Hybrid Entropy Weighted GRA-TOPSIS Method. *Process Integr. Optim. Sustain.* 6(1), 61–72. https://doi.org/10.1007/s41660- 021-00202-6.

[2] Bisariya, S.; Afzal, N. (2024). NSGA-II- and Fuzzy-TOPSIS Algorithms-Based Realization of a Low-Power and High-gm CDTA. *Int. J. Fuzzy Syst*. https://doi.org/10.1007/s40815-024-01908-8.

[3] Chen, P.; Huang, T.; Wu, B.; Qian, H.; Xie, F.; Liu, B.; Liu, D.; Li, X. (2024) Modeling the Discharge Rate of a Screw Conveyor Considering Hopper-Conveyor Coupling Parameters. *Agric.-Basel*, 14 (7). https://doi.org/10.3390/agriculture14071203.

[4] Dao, T.-P.; Huang, S.-C. (2015). Robust Design for a Flexible Bearing with 1-DOF Translation Using the Taguchi Method and the Utility Concept. *J. Mech. Sci. Technol*. 29 (8), 3309–3320. https://doi.org/10.1007/s12206-015-0728-3.

[5] Gheibollahi, H.; Masih-Tehrani, M. (2023). A Multi-Objective Optimization Method Based on NSGA-II Algorithm and Entropy Weighted TOPSIS for Fuzzy Active Seat Suspension of Articulated Truck Semi-Trailer. Proc. Inst. Mech. Eng. Part C-J. *Mech. Eng. Sci.* https://doi.org/10.1177/ 09544062231151799.

[6] Guacheta-Alba, J.C.; Nunez, D.A.; Dutra, M.S.; Mauledoux, M.; Aviles, O.F. (2023). Multi-Objective Optimization of 6-DOF Deposition Trajectories Using NSGA-II. *J. Braz. Soc. Mech. Sci. Eng*., 45 (11), 610. https://doi.org/10.1007/s40430-023-04495-1.

[7] Huang, S.; Hu, Y.; Li, F.; Jin, W.; Wu, B. (2020). Multi-objective Optimization of Mechanical Oil Extraction from Camellia Oleifera Seeds Using Kriging Regression and NSGA-II. *J. Food Process Eng*., 43 (12), e13549. https://doi.org/10.1111/jfpe.13549.

[8] Jiang, R.; Ci, S.; Liu, D.; Cheng, X.; Pan, Z. (2021). A Hybrid Multi-Objective Optimization Method Based on NSGA-II Algorithm and Entropy Weighted TOPSIS for Lightweight Design of Dump Truck Carriage. *Machines*, 9 (8), 156. https://doi.org/10.3390/machines9080156.

[9] Li, Y.; Liu, Y.; Li, S.; Qi, L.; Xie, J.; Xie, Q. (2022). A Novel Multi-Objective Optimal Design Method for Dry Iron Core Reactor by Incorporating NSGA-II, TOPSIS and Entropy Weight Method. *Energies*, 15 (19), 7344. https://doi.org/ 10.3390/en15197344.

[10] Ma, Y.; Xiao, Y.; Wang, J.; Zhou, L. (2022). Multicriteria Optimal Latin Hypercube Design-Based Surrogate-Assisted Design Optimization for a Permanent-Magnet Vernier Machine. *IEEE Trans. Magn*., 58 (2). https://doi.org/10.1109/TMAG. 2021.3079145.

[11] Ma, Z.; Wu, Z.; Li, Y.; Song, Z.; Yu, J.; Li, Y.; Xu, L. (2024). Study of the Grain Particle-Conveying Performance of a Bionic Non-Smooth-Structure Screw Conveyor. *Biosyst. Eng*., 238, 94–104. https://doi.org/10.1016/j.biosystemseng. 2024.01.005.

[12] Minglani, D.; Sharma, A.; Pandey, H.; Dayal, R.; Joshi, J. B.; Subramaniam, S. (2020). A Review of Granular Flow in Screw Feeders and Conveyors. *Powder Technol*. 366, 369–381. https://doi.org/10.1016/j.powtec.2020.02.066.

[13] Ou, Z.; Yin, Y.; Gao, F.; Zhu, L. (2025). A Novel Multi-Objective Optimization Framework for the Thermal Management System of High-Power Density Switching Power Supply. *Appl. Therm. Eng.*, 264, 125471. https://doi.org/10.1016/j. applthermaleng. 125471.

[14] Podder, B.; Biswas, A.; Saha, S. (2021). Multi-Objective Optimization of a Small Sized Solar PV-T Water Collector Using Controlled Elitist NSGA-II Coupled with TOPSIS. *Sol. Energy*, 230, 688–702. https://doi.org/10.1016/j.solener.2021.10.078.

[15] Shakouri, O.; Assad, M. E. H.; Açıkkalp, E. (2021). Thermodynamic Analysis and Multi-Objective Optimization Performance of Solid Oxide Fuel Cell–Ericsson Heat Engine–Reverse Osmosis Desalination. *J. Therm. Anal. Calorim*, 145(3), 1075-1090. https://doi.org/10.1007/s10973-020-10413-7.

[16] Silva, F.F.D.N.; Martins, D.L.; Doria Neto, A.D.; Rodrigues, M.A.F.; Da Mata, W. (2016). Optimization of the Oil Production Fields Submitted the Water Injection, Using the Algorithm NSGA-II. *IEEE Lat. Am. Trans*., 14 (9), 4166–4172. https://doi.org/10.1109/TLA.2016.7785948.

[17] Sun, H.; Ma, H., Zhao, Y. (2021) DEM Investigation on Conveying of Non-Spherical Particles in a Screw Conveyor. *Particuology*. Volume 65, pp.17-31. https://doi.org/10.1016/j.partic.2021.06.009

[18] Tian, Y.; Yuan, P.; Yang, F.; Gu, J.; Chen, M.; Tang, J.; Su, Y.; Ding, T.; Zhang, K.; Cheng, Q. (2018) Research on the Principle of a New Flexible Screw Conveyor and Its Power Consumption. *Appl. Sci*.-Basel, 8 (7). https://doi.org/10.3390/app8071038.

[19] Wang, D.; Jiang, R.; Wu, Y. (2016) A Hybrid Method of Modified NSGA-II and TOPSIS for Lightweight Design of Parameterized Passenger Car Sub-Frame. *J. Mech. Sci. Technol*., 30 (11), 4909–4917. https://doi.org/10.1007/s12206-016-1010-z.

[20] Yu, R.; Han, H.; Yang, C.; Luo, W. (2022) Optimal Design and Decision Making of an Air Cooling Channel with Hybrid Ribs Based on RSM and NSGA-II. *J. Therm. Anal. Calorim*, 147 (10), 5839–5854. https://doi.org/10.1007/s10973-021-10807-1.

[21] Zhang, Tao, Liu, Fei, Zhao, Manquan, Liu Yueqin, Li Fengli, Ma Qian, Zhang Yong, Zhou Peng (2017). Measurement of physical parameters of contact between soybean seed and seed metering device and discrete element simulation calibration [J]. *Journal of China Agricultural University*, 22(0 9): 86-92.

[22] Zhang, X.; Wang, R.; Wang, B.; Chen, J.; Wang, X. (2024) Parameter Calibration of Discrete Element Model of Wine Lees Particles. *Appl. Sci*., 14 (12), 5281. https://doi.org/10.3390/app14125281.

[23] Zhou Zhenhui. (2019) *Simulation Research on the Screw Conveying Characteristics of a New Type of Grain Screw Stacker Based on EDEM*. Master thesis, Wuhan University of Technology, Wuhan.

[24] Zhou, Z., Lin, Z., Ma, Y., Niu, J., Liu, J., Wang, X. (2025) Optimal Design of Colour Formulation Prediction for Cotton Fabrics Based on NSGA-II and TOPSIS. *Color. Technol*. 2025, 141 (1), 63–79. https://doi.org/10.1111/cote.12749.